ON THE VIBRATIONS OF PYRAMIDAL BEAMS WITH RECTANGULAR CROSS-SECTION AND APPLICATION TO UNSWEPT WINGS

by L. M. B. C. CAMPOS *and* A. C. MARTA[†]

(*Center for Aeronautical and Space Science and Technology, IDMEC, Instituto Superior Técnico, Universidade de Lisboa, Portugal*)

[Received 8 April 2020. Revised 10 November 2020. Accepted 10 November 2020]

Summary

The bending frequencies of an unswept wing are calculated based on the model of a beam clamped at the root and free at the tip. For a tapered wing with straight leading- and trailing-edges, the chord is a linear function of the span; the same linear function of the span applies to thickness, in the case of constant thickness-to-chord ratio. The latter is usually small, so that the beam differs from the more frequent cases of a conical beam with a circular cross-section or a prismatic beam with a square cross-section. Thus, the bending modes of a non-uniform beam are considered, with mass and area moment of inertia which are respectively quadratic and quartic functions of the span. There is no exact solution expressible in finite terms using elementary functions, and thus power series expansions are used. The bending frequencies are calculated for a delta wing and compared with a rectangular wing, with the same span, mean chord and thickness, mass density and Young's modulus. It is shown that the fundamental frequency is higher by a factor 4.96 for the delta wing; it is also shown that the general case of the tapered wing is intermediate between the delta and the rectangular wing. Lastly, the analytical results obtained for the bending modes are compared with numerical modal analyses of general tapered wing beams using high-fidelity finite-element model software.

1. Introduction

The representation of a wing as a beam of constant cross-section is adequate for a rectangular wing, with airfoil section and material properties constant along the span. Retaining the latter case of an homogeneous wing, but with non-uniform chord and/or thickness, the mass and area moment of inertia of the section vary along the span. Thus the model must be extended to a beam of non-uniform cross-section, for example, for a tapered unswept wing whose cross-sections are orthogonal to the mid-line. For a sweptback wing, whose cross-sections are not orthogonal to the line of centroids, a more sophisticated approach is needed, such as plate rather than beam theory. The model of a beam of variable cross-section applies to a delta wing and also to a truncated tapered wing. A particular case of tapered wing is the delta wing, for which the mass and area moment of inertia vanish at the tip. The study of beam bending in general, and its natural vibration frequency in particular, has been of interest since many years and it is a standard topic of elasticity, vibrations and aeroelasticity.

[†]<andre.marta@tecnico.ulisboa.pt>

Q. Jl Mech. Appl. Math, Vol. 74. No. 1 © The Author, 2021. Published by Oxford University Press; all rights reserved. For Permissions, please email: journals.permissions@oup.com. Advance Access publication 2 February 2021. doi:10.1093/qjmam/hbaa017

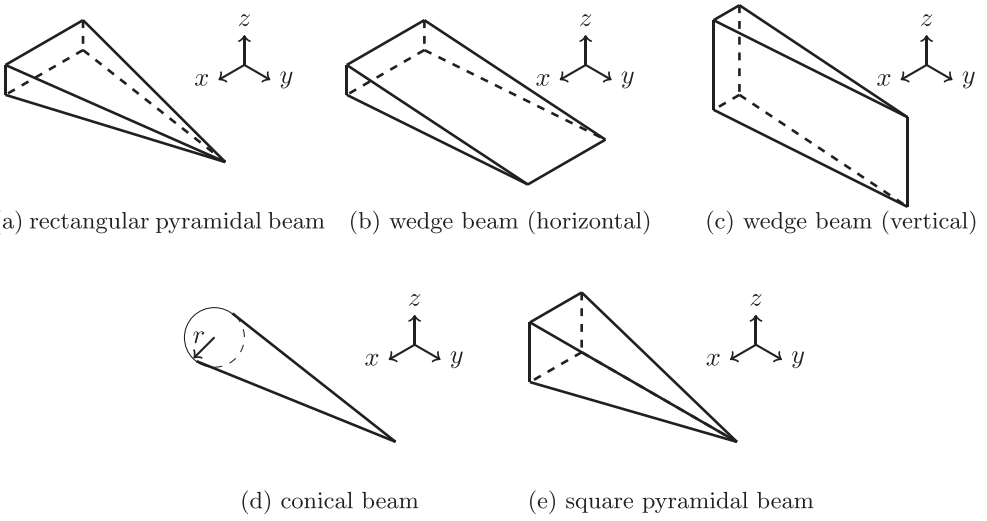

(a) rectangular pyramidal beam (b) wedge beam (horizontal) (c) wedge beam (vertical)

(d) conical beam (e) square pyramidal beam

Fig. 1 Comparison of different beam geometries with linearly varying cross-sections for vertical z vibrations.

This article considers the bending vibrations of a pyramidal beam (Fig. 1(a)) whose rectangular cross-section decreases linearly with axial distance y both in the vertical z and horizontal x directions. This is distinct from a wedge for which the rectangular cross-section is constant in one direction and decreases linearly with axial distance in the other direction; the horizontal wedge was considered for vertical z vibrations (Fig. 1(b)) by (**1**), and the vertical wedge was considered for vertical z vibrations (Fig. 1(c)) by (**2**). The wedge (Fig. 1(b) and (c)) applies only to wings with rectangular planform, whereas the pyramidal beam includes other shapes like the delta wing.

All of the preceding are particular cases of tapered beams, first considered by (**3**), in more detail for the conical beam with circular cross-section with radius r decreasing linearly with axial distance y up to the vertex (Fig. 1(d)). The closest analogue for a pyramidal beam is the case of square cross-section (Fig. 1(e)) decreasing linearly with axial distance y up to the vertex. In the case of a wing with span in the y direction, the chord $c(y)$ in the x direction is much larger than the thickness $e(y)$ in the z direction, and thus the cross-section is a slim rectangle, far from a square. The equations describing the vibrations of a beam of variable cross-section are compared in Appendix A for the horizontal (**1**) and vertical (**2**) wedges and for the present case of a rectangular pyramidal beam.

Thus, the vibrations of a pyramidal beam are distinct from those of other tapered beams, like wedges or cones, and more suited for application to wings, like the delta wing. The pyramidal beam may be truncated before the vertex, allowing for non-rectangular wings with non-sharp tips. The pyramidal beam model is used to obtain exact analytical solutions for the natural frequencies and modes of vibration of wings, in comparison with other approximate or numerical approaches mentioned next.

The transverse vibration of homogeneous Euler–Bernoulli beams with variable cross sections has received wide attention since Kirchhoff's work (**3**) where the fundamental frequency of cantilever conical beams with circular cross-section was first tackled. Since then, the study of non-uniform beams continued with emphasis on truncated beams and more general shaped beams. In the present

case, the beam differs significantly from a conical beam, in that the cross-section is rectangular, with the chord in one direction usually much larger than the thickness in the other direction. While many combinations of height and width variations are possible, it is common to consider a power function lengthwise. In any case, it results in a fourth order linear differential equation with variable coefficients and with a regular singularity, for which analytical solutions may be possible in terms of Bessel functions, hypergeometric functions or power series for a few particular types of non-uniform beams. In general, numerical methods based on Rayleigh–Ritz, Galerkin, finite difference and finite element procedures have been used to obtain an approximate solution.

In 1922, Wrinch (**4**) studied the lateral vibrations of conical beams, under the same clamped-free boundary conditions as Kirchhoff's work, where she used Bessel functions of the second and third kind to find the first three vibration modes of sharp ended (complete) conical beams. A few years later, Ono (**5**) pioneered the investigation of truncated beams, but assuming constant thickness and linear tapering width. He used an approximate methods, the Rayleigh's method, to solve the elastic line equation in integral form to estimate lower and upper bounds of the vibration frequencies. The analysis of frequencies of truncated cone cantilever beams subject to different boundary conditions was conducted by Conway *et al.* (**6**). Approximate methods of solutions were used where the Bessel functions were replaced by their polynomial approximations in the numerical evaluation of the determinant in the eigenvalue problem of the vibration differential equation. That work was later extended by Lau (**7**) to include an end mass on the tapered beam. Gaines and Volterra (**8**) presented numerical computations of the upper and lower natural frequencies for transverse vibrations for the first three natural frequencies of cone and wedge cantilever beams, both complete and truncated, using the approximate Rayleigh–Ritz method. Also around that time, Wang (**9**), still considering the differential equation for the mode functions of tapered vibrating beams using the Euler beam theory, presented the analytic solution as a linear combination of generalized hypergeometric functions (**10**), having also noted that they could also by obtained by the standard series method—the Frobenius method—as used in the work presented here. The obtained comprehensive numerical approximate solutions for natural frequencies and nodes for transverse vibration using a restricted number of terms in coefficients of the determinant, as here defined in (51), were summarized in tabular form for both complete and truncated beams, considering cross-section lengthwise variations of arbitrary powers, under different boundary conditions (**10**). Later, Sato (**11**) improved the Rayleigh–Ritz method in the study of transverse vibrations of linearly tapered beams under axial load with ends elastically supported.

Downs (**12**) extended the analysis of tapered beams considering not only the Euler theory but also the Timoshenko theory to account for significant shear deformation. Instead of the analytical approach followed by his predecessors, he used a numerical method similar to the finite element formulation but then employed a dynamic discretization technique that directly used the elastic properties of beam segments of variable length along the span and chord, resulting in high accuracy compared with exact solutions and other numerical results.

In spite of the development of powerful numerical approximation methods, the direct solution of the mode shape equations were still tough for other tapered beam cases. Naguleswaran (**2**) studied the analytic solution of the mode shape equation for the case of the Euler–Bernoulli beam of constant height and linearly varying width. The direct solution to the mode shape equation, based on the Frobenius method, was expressed as the superposition of four independent solution functions, three of which are power series and the fourth is a series with logarithmic terms. The roots of the resulting frequency equations, given by 2×2 and 4×4 determinants respectively for the complete (sharp end) and the truncated beams, were then evaluated numerically using an iterative method. Then,

Chen (13) numerically evaluated the natural vibration frequencies of a truncated beam, using the Runge-Kutta method to solve the analytic bending differential equation, subject to different boundary conditions. Amabili and Garziera (14) found solutions for a simply supported beam of rectangular cross-section of constant height and linearly varying width using the approximation Rayleigh–Ritz method. One year later, Zhou and Cheung (15) studied tapered beams with continuously varying rectangular cross-section of arbitrary power function using the same method. More recently, Bayat *et al.* (16) tackled the nonlinear, large amplitude, free vibration of tapered beams using the max–min approach and the homotopy perturbation method to quickly find approximate solutions. Later, using a similar numerical method to determine the natural frequencies, Wang (17) extended the study of the vibration of a cantilever beam with constant height and linearly tapered width to include tip mass and base flexibility.

The proper and detailed mechanical characterization of the tapered cantilever beam is fundamental for many structural applications, in particular aircraft wings, whose complex structure can be idealized as a tapered beam. The accurate study of the aeroelastic response of wings, being them fixed as in aircraft or rotating as in helicopters, is of major relevance regarding not only flight dynamics and stability but also vibration and fatigue. This is even more important as more and more flexible structures are being used, often made of composite materials.

The study of flexible aircraft wings is often made by means of beam finite elements, where a modal analysis identifies the natural frequencies (eigenvalues) and vibration modes (eigenmodes), using nonlinear elements (18) and coupled bending-torsion (19). The coupled nonlinear flight dynamics and aeroelasticity of highly flexible flying wings have also been tackled by means of finite element formulation (20) dealing with complex phenomena such as variable wing torsional stiffness due to skin wrinkling and unsteady aerodynamics with stall models. A similar problem have also been solved in the frequency domain using the fully coupled linearized formulation around aeroelastic trim conditions, with a state-space representation including rigid-body, elastic and aerodynamic variables (21).

The study of physical phenomena involving any combination of solid mechanics, dynamics and fluid mechanics are becoming more and more recurrent in aerospace, namely in the study of airplanes. For example, the usage of an aeroelastic analytical model for the bending-torsion dynamics of a slender high aspect-ratio wing in inviscid subsonic airflow, that comprised both a cantilever beam model as structural model and a potential field model as linear aerodynamic model, to study the aeroelastic modes and flutter instability in two-dimensions (22). When considering the full three-dimensional effects in flexible wing configurations, it is necessary to consider both aeroelasticity and flight dynamics coupled, as the frequencies of rigid-body motions and elastic modes are closer (23).

Regarding helicopter blades, the accurate prediction of the natural frequencies and mode shapes are critical to ensure that resonance conditions due to the periodic passage by the fuselage are avoided, and multibody dynamics is typically used in these cases (24). The helicopter blades are often modelled as cantilever rotating beams and, for some particular classes, exact solutions exist which are expressed in terms of hypergeometric functions (25). For general classes, only approximate solutions exist, such as those found using the Rayleigh–Ritz method for rotating cantilever beams (26) and rotating tapered beams with attached inertia elements (27).

Analytical studies of mechanical vibration problems, regardless of the simplifications often deemed necessary to obtain approximate solutions, constitute an important knowledge base. There are already many approximate analytical solutions available, including cases as diverse as simple supported composite and sandwich plates (28), cracked beams in bending (29), nonlinear functionally graded plates (30) and beams (31), and carbon nanotubes using beam models (32) or shell models (33).

As such, the knowledge of exact analytical solutions of dynamic response of rather simplistic wing structures offers valuable data. It can be used as benchmark to validate high-fidelity computational fluid-structure interaction models, that upon validation, can then be used to tackle complex wing configurations. The work presented here intends to provide such reference data for tapered wings and can be seen as an extension to the work by Naguleswaran (**2**), where the direct solution to the mode shape equation based on the Frobenius method is given for a linearly tapered beam, in both width and height, including the limit cases of delta (complete sharp ended) and rectangular planforms, as well as any general intermediate planform case (truncated beam).

The Frobenius power series has already seen usage in the solution of several mechanical problems governed by linear differential equations that are regular in the neighbourhood of a singular point, for which solutions based on Bessel function do not exist, assuming a set of specific material or geometry conditions. Examples include the free vibrations of infinitely long orthotropic solid and hollow cylinders (**34**), the propagation of cylindrical waves in composite cylinders made of homogeneous coaxial layers (**35**), radially inhomogeneous materials with arbitrary cylindrical anisotropy (**36**), rotating inclined beams (**37**) and stress analysis in thick-walled functionally graded cylindrical pressure cylinders assuming radial exponential material properties for the stationary (**38**) and rotating (**39**) cases. Power series have also been used in the study of the dynamic response of non-uniform rotating Euler–Bernoulli wedge and cone beams with rotational and flexible ends (**40**).

This article is divided into seven main sections. Section 2 lays out a few basic geometric and physical function definitions for straight leading- and trailing-edges wings. The equation of transverse vibrations is applied to such wings and general expressions of amplitude and frequency of oscillation are derived in section 3. The analytical solution of natural bending frequency of tapered wings, in the form of an eigenvalue problem, is determined in section 4, while the particular cases of rectangular and delta wings are included in sections 5 and 6, respectively. The dimensionless frequency is evaluated for general tapered wings in section 7. In section 8, the analytical solutions are compared with some numerical finite-element models. The article ends with some remarks about the use of exact analytical solutions versus finite element numerical methods.

2. Spanwise distribution of mass and area moment of inertia

Different wing configurations can be found in aircraft design, depending on the flight characteristics, such as rectangular, elliptic, tapered, delta, trapezoidal or swept wings. This work focuses on unswept tapered wings with straight leading- and trailing-edges, as represented in Fig. 2. A Cartesian reference frame with y along the span, x along the chord $c(y)$ and z along the thickness $e(y)$ is used; the latter specifies for a given mass density $\rho(y)$, the mass per unit length $m(y)$ and the moment of inertia of the cross-section $I(y)$ used in the non-uniform beam model of the wing.

In the case of a tapered unswept wing with straight leading and trailing edges in Fig. 2, the chord at spanwise section y is given by

$$c(y) = c_r + (c_t - c_r)\frac{y}{L}, \quad 0 \le y \le L, \tag{1a, b}$$

where L is the semi-span and c_r, c_t are the chord at the root and tip, respectively. The latter are related to the mean chord (1c), and taper ratio (1d),

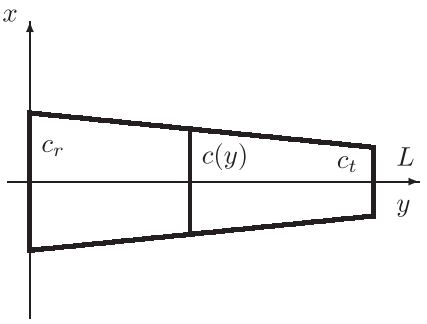

Fig. 2 Planform view of (unswept) tapered wing with straight leading- and trailing-edges, with semi-span L, root chord c_r and tip chord c_t.

$$\bar{c} = \frac{c_r + c_t}{2}\,, \quad 0 \leq \lambda \equiv \frac{c_t}{c_r} \leq 1\,, \tag{1c, d}$$

leading to

$$c(y) = \frac{2\bar{c}}{1+\lambda}\left[1 + (\lambda - 1)\frac{y}{L}\right], \tag{2}$$

as the function of the spanwise coordinate. If the wing sections have a constant thickness-to-chord ratio, then (2) also applies to the thickness distribution along the span,

$$e(y) = \frac{2\bar{e}}{1+\lambda}\left[1 + (\lambda - 1)\frac{y}{L}\right], \tag{3}$$

where $\bar{e}$ is the mean thickness; in such case, the thickness-to-chord ratio is $e(y)/c(y) = \bar{e}/\bar{c} = \text{const}$. Using the expressions (2) and (3) results for the wing cross-sectional area,

$$A(y) = c(y)e(y) = A_0\left[1 + (\lambda - 1)\frac{y}{L}\right]^2\,, \quad A_0 = \frac{4\bar{c}\bar{e}}{(1+\lambda)^2}\,. \tag{4}$$

Assuming that the section is homogeneous with mass density ρ, the mass per unit span is given by a quadratic function (5) using the expression (4),

$$m(y) = \rho\, A(y) = m_0\left[1 + (\lambda - 1)\frac{y}{L}\right]^2\,, \tag{5a}$$

$$m_0 \equiv m(0) = \rho A_0 = \frac{4\rho\bar{c}\bar{e}}{(1+\lambda)^2}\,, \tag{5b}$$

where m_0 would be the constant value for a rectangular wing. Likewise, the area moment of inertia per unit span relative to the z-axis, for a rectangle with height equal to the mean thickness of the airfoil $e(y)$ and length equal to the chord $c(y)$, as illustrated in Fig. 3, is given by

$$I(y) = \frac{1}{12}c(y)\left[e(y)\right]^3\,. \tag{6}$$

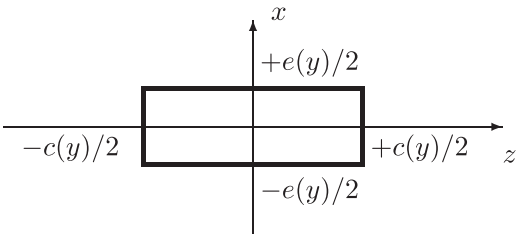

Fig. 3 Arbitrary cross-section at spanwise position y with height equal to the mean thickness of the airfoil $e(y)$ and length equal to the chord $c(y)$.

Substituting (2) and (3) in (6) leads to a quartic function (7a),

$$I(y) = I_0 \left[1 + (\lambda - 1)\frac{y}{L}\right]^4 , \quad I_0 \equiv I(0) = \frac{4}{3}\frac{\bar{c}\bar{e}^3}{(1+\lambda)^4} , \tag{7a, b}$$

where (7b) would be the constant value for a rectangular wing. The Kirchhoff conical beam (**3**) corresponds to the linearly tapered wing with thickness equal to chord, specifying the radius of the cross-section $e(y) = c(y) = r(y)$, mass per unit length $m(y) = \rho\pi\,[r(y)]^2$ and area moment of inertia $I(y) = \frac{\pi}{4}[r(y)]^4$.

3. Transverse vibrations of beam with non-uniform cross-section

The transverse or vertical displacement $X(y, t)$ of an elastic beam, with Young's modulus $E(y)$, mass per unit span $m(y)$ and area moment of inertia $I(y)$, satisfies the equation of bending waves,

$$-m(y)\frac{\partial^2 X(y,t)}{\partial t^2} = \frac{\partial^2}{\partial y^2}\left[E(y)I(y)\frac{\partial^2 X(y,t)}{\partial y^2}\right] . \tag{8}$$

For a homogeneous wing, the Young's modulus is constant, and for a tapered wing with straight leading- and trailing-edges and constant thickness-to-chord ratio, the substitution of the mass (5) and area moment of inertia (7) in (8) leads to the linear partial differential equation with non-uniform coefficients,

$$-\left[1 + (\lambda - 1)\frac{y}{L}\right]^2 \frac{\partial^2 X(y,t)}{\partial t^2} = \frac{EI_0}{m_0}\frac{\partial^2}{\partial y^2}\left\{\left[1 + (\lambda - 1)\frac{y}{L}\right]^4 \frac{\partial^2 X(y,t)}{\partial y^2}\right\} . \tag{9}$$

Since the coefficients do not depend on time, there are sinusoidal oscillations with frequency ω expressed as

$$X(y, t) = F(y)\cos(\omega t) , \tag{10}$$

whose amplitude satisfies a linear ordinary differential equation with variable coefficients,

$$\frac{d^2}{dy^2}\left\{\left[1 + (\lambda - 1)\frac{y}{L}\right]^4 \frac{d^2F(y)}{dy^2}\right\} - \frac{\omega^2 m_0}{EI_0}\left[1 + (\lambda - 1)\frac{y}{L}\right]^2 F(y) = 0 . \tag{11}$$

The change of independent variable, with $\lambda \neq 1$,

$$\xi \equiv 1 + (\lambda - 1)\frac{y}{L}\,, \quad F(y) \equiv G(\xi)\,, \tag{12a, b}$$

implies (12c,d),

$$0 \leq \xi < 1\,, \quad \frac{d}{dy} = \frac{\lambda - 1}{L}\frac{d}{d\xi} \tag{12c, d)}\,,$$

and transforms the coefficients in (11) to powers in (13),

$$\frac{d^2}{d\xi^2}\left[\xi^4 \frac{d^2 G}{d\xi^2}\right] - \Omega^2 \xi^2 G = 0\,, \tag{13}$$

where the only parameter is the dimensionless frequency,

$$\Omega \equiv \frac{\omega L^2}{(\lambda - 1)^2}\sqrt{\frac{m_0}{EI_0}} = \frac{\omega L^2}{\bar{e}}\sqrt{\frac{3\rho}{E}}\frac{\lambda + 1}{(\lambda - 1)^2}\,, \tag{14a}$$

which involves the frequency of oscillation ω, material properties through the Young's modulus E and density ρ, and wing geometry through the semi-span L, mean thickness $\bar{e}$ and taper ratio λ. It should be noted that the usual form of the eigen or characteristic value considers the properties at the cantilever end, for example, the wing root,

$$\widetilde{\Omega} \equiv \omega L^2 \sqrt{\frac{m_0}{EI_0}} = \frac{\omega L^2}{\bar{e}}\sqrt{\frac{3\rho}{E}}(\lambda + 1)\,, \tag{14b}$$

thus holding the relationship

$$\widetilde{\Omega} = \Omega(\lambda - 1)^2\,. \tag{14c}$$

As such, the results presented in sections 6–8 will include both definitions (14a) and (14b) to allow for the direct comparison with previous results found in the literature.

Upon the expansion of (13), the resulting linear fourth-order ordinary differential equation with power coefficients (15),

$$\xi^4 G'''' + 8\xi^3 G''' + 12\xi^2 G'' - \Omega^2 \xi^2 G = 0\,, \tag{15}$$

has no exact solution which can be expressed in finite terms using only elementary functions. Since the only singularities are $\xi = 0, \infty$, and $\xi = 0$ is a regular singularity, there are solutions (16) as Frobenius–Fuchs series (**41**),

$$G_\sigma(\xi) = \sum_{n=0}^{\infty} a_n(\sigma)\xi^{n+\sigma}\,, \tag{16}$$

which has infinite radius of convergence, $0 < \xi < \infty$, and thus covers the region of interest $\lambda \leq \xi \leq 1$ in (12a) corresponding to $0 \leq y \leq L$. Thus the solution (16) will be needed at most only in the unit interval $0 \leq \xi \leq 1$, in the case of the delta wing with zero taper ratio ($\lambda = 0$) and tip chord ($c_t = 0$).

Substituting the Frobenius–Fuchs series (16) in the differential equation (15), and equating to zero the coefficients of the powers of ξ, leads to the recurrence formula:

$$(n+\sigma)(n+\sigma-1)[12+(n+\sigma-2)(n+\sigma+5)]a_n(\sigma)-\Omega^2 a_{n-2}(\sigma)=0\,. \tag{17}$$

Note that (17) implies that the coefficients decay like $a_n \sim o(n^{-4})$, ensuring the uniform and absolute convergence of the series (16) for finite $\xi < \infty$.

Substituting the series (16) with the recurrence formula for the coefficients (17) in the differential equation (15) leaves only the lowest order $n = 0$ term,

$$\left\{\mathcal{L}\left(\frac{\mathrm{d}}{\mathrm{d}\xi}\right)\right\} G_\sigma(\xi)=[(\sigma-1)\sigma(\sigma+1)(\sigma+2)]\,a_0(\sigma)\,, \tag{18}$$

where the non-uniform bending operator (19) is linear,

$$\mathcal{L}\left(\frac{d}{d\xi}\right)=\xi^4\frac{d^4}{d\xi^4}+8\xi^3\frac{d^3}{d\xi^3}+12\xi^2\frac{d^2}{d\xi^2}-\Omega^2\xi^2\,. \tag{19}$$

The coefficient (20a) cannot be zero, otherwise by (17) all coefficients would vanish and by (16) a trivial solution would result. Thus a non-trivial (20a) solution (20b) is possible only for the four values of the index (20c–f) that are roots of the term in square brackets on the r.h.s. of (18),

$$a_0(\sigma)\neq 0=\left\{\mathcal{L}\left(\frac{d}{d\xi}\right)\right\} G_\sigma(\xi):\sigma_1=1,\sigma_2=0,\sigma_3=-1,\sigma_4=-2. \tag{20a-f}$$

To each index (20c–f) corresponds a linearly independent particular integral, and the general integral is their linear combination,

$$G(\xi)=C_1H_1(\xi)+C_2H_2(\xi)+C_3H_3(\xi)+C_4H_4(\xi)\,, \tag{21}$$

with arbitrary constants C_1, C_2, C_3 and C_4. The constants $a_0(\sigma_n)$ may be incorporated in the C_n, and thus set to unity (22ca) when using (17) in (22cb,c),

$$a_0(\sigma)=1: \tag{22a}$$

$$a_n(\sigma)=\frac{\Omega^2}{f_n(\sigma)}a_{n-2}(\sigma)\,, \tag{22b}$$

$$f_n(\sigma)=(n+\sigma+2)(n+\sigma+1)(n+\sigma)(n+\sigma-1)\,. \tag{22c}$$

Using (22cb,c) by recurrence specifies all coefficients of even order,

$$a_{2n}(\sigma)=\frac{\Omega^{2n}}{f_{2n}(\sigma)f_{2n-2}(\sigma)..f_2(\sigma)} \tag{23a}$$

$$=\frac{\Omega^{2n}}{[(2n+\sigma+2)(2n+\sigma+1)(2n+\sigma)^2(2n+\sigma-1)^2...(\sigma+4)^2(\sigma+3)^2(\sigma+2)(\sigma+1)]}\,. \tag{23b}$$

The coefficients (23b) are all finite for the largest index (20c) leading (16) to the first particular integral (24a),

$$H_1(\xi) \equiv G_1(\xi) = \sum_{n=0}^{\infty} \frac{\Omega^{2n}\xi^{2n+1}}{(2n+3)(2n+2)(2n+1)^2(2n)^2 ... 5^2 \cdot 4^2 \cdot 3 \cdot 2} = O(\xi)\,, \tag{24a,b}$$

that is a function of the first kind specified by a power series (24b). The coefficients (23b) are also all finite for the second largest index (20d) leading (16) to another particular integral (25a),

$$H_2(\xi) \equiv G_0(\xi) = \sum_{n=0}^{\infty} \frac{\Omega^{2n}\xi^{2n}}{(2n+2)(2n+1)(2n)^2(2n-1)^2 ... 4^2 \cdot 3^2 \cdot 2 \cdot 1} = O(1)\,. \tag{25a,b}$$

Substituting (22ca,23b) in (16), the leading terms are

$$\begin{aligned} G_\sigma(\xi) = \xi^\sigma \Bigg\{ 1 &+ \frac{\Omega^2\xi^2}{(\sigma+1)(\sigma+2)(\sigma+3)(\sigma+4)} + \\ &+ \frac{\Omega^4\xi^4}{(\sigma+1)(\sigma+2)(\sigma+3)^2(\sigma+4)^2(\sigma+5)(\sigma+6)} + ... \\ &+ \frac{\Omega^{2n}\xi^{2n}}{(\sigma+1)(\sigma+2)(\sigma+3)^2(\sigma+4)^2 ... (\sigma+2n-1)^2(\sigma+2n)^2(\sigma+2n+1)(\sigma+2n+2)} ... \Bigg\}\,. \end{aligned} \tag{26}$$

It can be checked that (26) leads to (24a) for the index $\sigma = 1$ in (20c) and to (25a) for the index $\sigma = 0$ in (20d). For the index $\sigma = -1$ in (20e) all terms in (26) have a simple pole since $\sigma + 1 = 0$ in the denominator. The pole is removed multiplying the coefficients (27a) by $\sigma + 1$ so that the new solution (27b),

$$\overline{a}_n(\sigma) = (\sigma+1)a_n(\sigma)\,, \qquad \overline{G}_\sigma(\xi) = \sum_{n=0}^{\infty} \xi^{n+\sigma}\overline{a}_n(\sigma)\,, \tag{27a,b}$$

satisfies (18) with the extra factor $\sigma + 1$ on the r.h.s. leading to (28),

$$\left\{\mathcal{L}\left(\frac{d}{d\xi}\right)\right\}\overline{G}_\sigma(\xi) = (\sigma-1)\sigma(\sigma+1)(\sigma+2)\overline{a}_0(\sigma) \tag{28a}$$

$$= (\sigma-1)\sigma(\sigma+1)^2(\sigma+2)a_0(\sigma)\,. \tag{28b}$$

To the index (20e) correspond two (29b,c) solutions (29a),

$$\left\{\mathcal{L}\left(\frac{d}{d\xi}\right)\right\}\overline{G}_\sigma(\xi) = 0 \;:\quad \lim_{\sigma\to-1}\left\{\overline{G}_\sigma(\xi), \frac{\partial}{\partial\sigma}\left[\overline{G}_\sigma(\xi)\right]\right\}\,. \tag{29a-c}$$

The first solution (29b) starts with the power $\xi^{\sigma_1+1} = \xi^0 = 1$ and coincides with (25a). The second solution (29c) provides a particular integral,

$$\overline{G}_{-1}(\xi) = \lim_{\sigma\to-1}\frac{\partial}{\partial\sigma}\left[(\sigma+1)G_\sigma(\xi)\right] = \lim_{\sigma\to-1}\frac{\partial}{\partial\sigma}\left[(\sigma+1)\sum_{n=0}^{\infty}\xi^{2n+\sigma}a_{2n}(\sigma)\right]\,. \tag{30a,b}$$

that is shown next to be linearly independent from (24a) and (25a). Substituting (23b) in (30b) leads to

$$H_3(\xi) \equiv \overline{G}_{-1}(\xi) = \lim_{\sigma\to -1} \frac{\partial}{\partial\sigma} \left\{ (\sigma+1) \sum_{n=0}^{\infty} \Omega^{2n} \xi^{2n+\sigma} \left[(2n+\sigma+2)(2n+\sigma+1) \right.\right.$$
$$\left.\left. (2n+\sigma)^2 (2n+\sigma-1)^2 ... (\sigma+4)^2 (\sigma+3)^2 (\sigma+2)(\sigma+1) \right]^{-1} \right\} . \quad (31)$$

The factor $\sigma+1$ in the numerator cancels with the same factor $\sigma+1$ in the denominator, except for the first term $n=0$, so now the limit $\sigma \to -1$ exists,

$$H_3(\xi) = \lim_{\sigma\to -1} \frac{\partial}{\partial\sigma} \left\{ (\sigma+1)\xi^{\sigma} \sum_{n=1}^{\infty} \Omega^{2n} \xi^{2n} \left[(2n+\sigma+2)(2n+\sigma+1) \right.\right.$$
$$\left.\left. (2n+\sigma)^2 (2n+\sigma-1)^2 ... (\sigma+4)^2 (\sigma+3)^2 (\sigma+2) \right]^{-1} \right\} . \quad (32)$$

Differentiating the power leads to a logarithmic term (33a) and differentiation of the inverse powers leads to (33b),

$$\frac{\partial}{\partial\sigma} \left(\xi^{\sigma} \right) = \xi^{\sigma} \log \xi \, , \qquad \frac{\partial}{\partial\sigma} \left(\frac{1}{\kappa+\sigma} \right) = -\frac{1}{(\kappa+\sigma)^2} \, . \quad (33a,b)$$

In the first term of the r.h.s. of (32), the differentiation must be applied to $(\sigma+1)$ otherwise it gives zero,

$$\lim_{\sigma\to -1} \frac{\partial}{\partial\sigma} \left[(\sigma+1)\xi^{\sigma} \right] = \lim_{\sigma\to -1} \xi^{\sigma} \left[1 + (\sigma+1)\log\xi \right] = \lim_{\sigma\to -1} \xi^{\sigma} = \frac{1}{\xi} \, ; \quad (34)$$

using (34) for the first term on the r.h.s. of (32), and applying (33a,b) to the remaining leads to

$$H_3(\xi) = \frac{1}{\xi} + \lim_{\sigma\to -1} \xi^{\sigma} \sum_{n=1}^{\infty} \Omega^{2n} \xi^{2n} \left[(2n+\sigma+2)(2n+\sigma+1) \right.$$
$$\left. (2n+\sigma)^2 (2n+\sigma-1)^2 ... (\sigma+4)^2 (\sigma+3)^2 (\sigma+2) \right]^{-1}$$
$$\left\{ \log\xi - \frac{1}{2n+\sigma+2} - \frac{1}{2n+\sigma+1} - \frac{2}{2n+\sigma} \right.$$
$$\left. - \frac{2}{2n+\sigma-1} ... - \frac{2}{\sigma+4} - \frac{2}{\sigma+3} - \frac{1}{\sigma+2} \right\} ; \quad (35)$$

The third particular integral is thus (36a),

$$H_3(\xi) = \frac{1}{\xi} + \sum_{n=1}^{\infty} \Omega^{2n} \xi^{2n-1} \left[(2n+1)(2n)(2n-1)^2 (2n-2)^2 ... 3^2 \cdot 2^2 \cdot 1 \right]^{-1}$$

$$\left\{\log\xi-\frac{1}{2n+1}-\frac{1}{2n}-\frac{2}{2n-1}-\frac{2}{2n-2}\ldots-\frac{2}{3}-\frac{2}{2}-\frac{1}{1}\right\}=O(\xi^{-1})\,. \tag{36a, b}$$

The particular integral (36a) has a simple pole (36b) and thus is linearly independent from (24a,b) and (25a,b). A similar analysis applies to the fourth index (20f) leading to

$$H_4(\xi)\equiv\overline{G}_{-2}(\xi)=\lim_{\sigma\to-2}\frac{\partial}{\partial\sigma}\left\{(\sigma+2)\xi^\sigma+\sum_{n=1}^{\infty}\Omega^{2n}\xi^{2n}\left[(2n+\sigma+2)(2n+\sigma+1)\right.\right.$$
$$\left.\left.(2n+\sigma)^2(2n+\sigma-1)^2\ldots(\sigma+4)^2(\sigma+3)^2(\sigma+1)\right]^{-1}\right\}. \tag{37}$$

An evaluation similar to (33a,b;34;35;36a,b) leads to

$$H_4(\xi)=\frac{1}{\xi^2}+\sum_{n=1}^{\infty}\Omega^{2n}\xi^{2n-2}\left[(2n)(2n-1)(2n-2)^2(2n-3)^2\ldots2^2\cdot1^2\cdot(-1)\right]^{-1}$$

$$\left\{\log\xi-\frac{1}{2n}-\frac{1}{2n-1}-\frac{2}{2n-2}-\frac{2}{2n-3}\ldots-\frac{2}{2}-\frac{2}{1}-\frac{1}{-1}\right\}=O(\xi^{-2})\,, \tag{38a, b}$$

that has a double pole. The leading terms in (24b,25b,36b,38b) confirm that the four particular integrals (24a,25a,36a,38a) in the general integral (21) are linearly independent. The first two integrals (24a,b;25a,b) are functions of the first kind and the last two (36a,b;38a,b) functions of the second kind, respectively with a simple and a double pole.

The two solutions of the first kind (24a) and (25a) involve only factorials,

$$H_1(\xi)=3!\xi\sum_{n=0}^{\infty}\frac{(\Omega\,\xi)^{2n}}{(2n+3)!(2n+1)!}\,, \tag{39}$$

$$H_2(\xi)=2!\sum_{n=0}^{\infty}\frac{(\Omega\,\xi)^{2n}}{(2n+2)!(2n)!}\,, \tag{40}$$

that are particular cases of the Gamma function (**42**). The Digamma function (**42**),

$$\psi(1+\nu+n)-\psi(1+\nu)=\sum_{m=1}^{n}\frac{1}{\nu+m}\,, \tag{41}$$

appears in the two solutions (36a) and (38a) of the second kind,

$$H_3(\xi)=\frac{1}{\xi}\left\{1+\sum_{n=1}^{\infty}\frac{(\Omega\,\xi)^{2n}}{(2n+1)!(2n-1)!}\left[\log\xi-\psi(2n+2)+\psi(2)-\psi(2n)+\psi(1)\right]\right\}, \tag{42}$$

$$H_4(\xi) = \frac{1}{\xi^2}\left\{1 - \sum_{n=1}^{\infty} \frac{(\Omega\,\xi)^{2n}}{(2n)!(2n-2)!}\left[\log\xi - \psi(2n+1) + \psi(2) - \psi(2n-1) + \psi(1)\right]\right\}. \tag{43}$$

Substituting $n = m + 1$, the sum in m starts at $m = 0$ leading to

$$\begin{aligned} H_3(\xi) =& \frac{1}{\xi}\left\{1 + \sum_{m=0}^{\infty} \frac{(\Omega\,\xi)^{2m+2}}{(2m+3)!(2m+1)!}\left[\log\xi - \psi(2m+4) + \psi(2) - \psi(2m+2) + \psi(1)\right]\right\} \\ =& \frac{1}{\xi} + \frac{\Omega^2}{3!}\log\xi\cdot G_1(\xi) - \Omega\sum_{n=0}^{\infty} \frac{(\Omega\,\xi)^{2n+1}}{(2n+3)!(2n+1)!}\left[\psi(2n+4) - \psi(2) + \psi(2n+2) - \psi(1)\right], \end{aligned} \tag{44}$$

$$\begin{aligned} H_4(\xi) =& \frac{1}{\xi^2}\left\{1 - \sum_{m=0}^{\infty} \frac{(\Omega\,\xi)^{2m+2}}{(2m+2)!(2m)!}\left[\log\xi - \psi(2m+3) + \psi(2) - \psi(2m+1) + \psi(1)\right]\right\} \\ =& \frac{1}{\xi^2} + \frac{\Omega^2}{2!}\log\xi\cdot G_2(\xi) - \Omega^2\sum_{n=0}^{\infty} \frac{(\Omega\,\xi)^{2n}}{(2n+2)!(2n)!}\left[\psi(2n+3) - \psi(2) + \psi(2n+1) - \psi(1)\right]. \end{aligned} \tag{45}$$

Thus the solutions of the second kind (44,45) equal the sum of: (i) the solutions of the first kind (39) and (40) multiplied by a logarithm; (ii) a complementary function involving Digamma functions. The term $\psi(2)$ in square brackets in (42) and (43) can be omitted because it is a constant times (39) and (40), and can be incorporated in the arbitrary constants C_1 and C_2 in (21). In conclusion, the general solution (21) of the differential equation (13)≡(15) is a linear combination (21)≡(46b) of four functions, namely two of the first (39,40) and two of the second (44,45) kind,

$$a_0(\sigma_m) = 1 : G(\xi) = \sum_{m=1}^{4} C_m H_m(\xi), \tag{46a,b}$$

where the arbitrary constants in (46b) are determined by boundary conditions, and incorporate the coefficients (46a) that can be set to unity (22ca).

4. Clamped-free boundaries and natural frequencies

The general solution (46b) must satisfy boundary conditions, which will specify the natural frequencies. The four boundary conditions are determined by setting the beam:

(i) clamped at the root $y = 0$, $\xi = 1$, that is, zero displacement (47a) and slope (47b):

$$I: \quad X(0,t) = 0 \qquad \Rightarrow F(0) = 0 \quad \Rightarrow G(1) = 0, \tag{47a}$$

$$II: \quad \frac{\partial X(0,t)}{\partial y} = 0 \qquad \Rightarrow F'(0) = 0 \quad \Rightarrow G'(1) = 0; \tag{47b}$$

where the definitions (10) and (12a) have been used.

(ii) free at the tip $y = L$, $\xi = \lambda$, that is, zero bending moment (48a) and transverse force (48b):

$$III: \quad M(y \to L) = \lim_{y \to L} EI(y) \frac{\partial^2 X(y,t)}{\partial y^2} = 0$$

$$\Rightarrow \lim_{\xi \to \lambda} h(\xi) G''(\xi) = 0 \,, \tag{48a}$$

$$IV: \quad V(y \to L) = \frac{\partial M}{\partial y} = \lim_{y \to L} \frac{\partial}{\partial y} \left[EI(y) \frac{\partial^2 X}{\partial y^2} \right] = 0$$

$$\Rightarrow \lim_{\xi \to \lambda} \frac{\lambda - 1}{L} \frac{d}{d\xi} \left[h(\xi) G''(\xi) \right] = 0 \,, \tag{48b}$$

where

$$h(\xi) = EI_0 \xi^4 \left(\frac{d\xi}{dy} \right)^2 = \frac{4 \bar{c} \bar{e}^3}{3} E \left(\frac{\xi}{1+\lambda} \right)^4 \left(\frac{\lambda - 1}{L} \right)^2 . \tag{48c}$$

In addition to the definitions mentioned above, (7b) has also been used.

The boundary conditions at the wing root (47a,b) readily apply to (46b),

$$I: \quad G(1) = \sum_{m=1}^{4} C_m H_m(1) = 0 \,, \tag{49a}$$

$$II: \quad G'(1) = \sum_{m=1}^{4} C_m H'_m(1) = 0 \,. \tag{49b}$$

Concerning the boundary conditions (48a,b) at the wing tip $\xi \to \lambda$, the case of the delta wing $\lambda = 0$ will be excluded (it will be addressed subsequently in section 6), so that

$$III: \quad \lim_{\xi \to \lambda} h(\xi) G''(\xi) = h(\lambda) G''(\lambda) = h(\lambda) \sum_{m=1}^{4} C_m H''_m(\lambda) = 0 \,, \tag{50a}$$

$$IV: \quad \lim_{\xi \to \lambda} \frac{\lambda - 1}{L} \frac{d}{d\xi} \left[h(\xi) G''(\xi) \right] = \frac{\lambda - 1}{L} h(\lambda) \sum_{m=1}^{4} C_m H'''_m(\lambda) = 0 \,; \tag{50b}$$

in the derivation of

$$\lim_{\xi \to \lambda} \frac{d}{d\xi} \left[h(\xi) G''(\xi) \right] = h(\lambda) \sum_{m=1}^{4} C_m H'''_m(\lambda) + h'(\lambda) \sum_{m=1}^{4} C_m H''_m(\lambda) = 0 \,, \tag{50c}$$

the last term vanishes by (50a), and thus (50c) reduces to (50b). The four boundary conditions (49a,b) and (50a,b) form a linear homogeneous system of equations in $(C_1, C_2, C_3, C_4) \neq (0, 0, 0, 0)$, which cannot be all zero. Hence the determinant of coefficients must vanish,

$$\begin{vmatrix} H_1(1) & H_2(1) & H_3(1) & H_4(1) \\ H'_1(1) & H'_2(1) & H'_3(1) & H'_4(1) \\ H''_1(\lambda) & H''_2(\lambda) & H''_3(\lambda) & H''_4(\lambda) \\ H'''_1(\lambda) & H'''_2(\lambda) & H'''_3(\lambda) & H'''_4(\lambda) \end{vmatrix} = 0 \,. \tag{51}$$

For fixed variable $\xi = 1$ or $\xi = \lambda$, the particular solutions (39,40,44,45) depend through the coefficients (17) only on the dimensionless frequency defined by (14a). Thus, for each taper ratio λ, the roots of the determinant (51) specify the natural frequencies $\Omega_n(\lambda)$, of which the real root with smaller modulus is the fundamental frequency $\Omega_1(\lambda)$.

Before proceeding to calculate the natural frequencies, the case of the delta wing $\lambda = 0$, excluded from (50a,b), is considered. The two boundary conditions at the wing root (47a,b) are unchanged (49a,b) for the delta wing, but at the wing tip, the condition of zero bending moment (48a) leads to

$$III: \quad \lim_{\xi\to 0} h(\xi) H_m''(\xi) = \lim_{\xi\to 0} h(\xi) \frac{d^2}{d\xi^2} \sum_{n=0}^{\infty} a_n(\sigma_m) \xi^{n+\sigma_m}$$

$$\sim \lim_{\xi\to 0} \xi^4 \frac{d^2}{d\xi^2} \xi^{\sigma_m} = \lim_{\xi\to 0} \sigma_m(\sigma_m - 1) \xi^{\sigma_m+2} = 0\,, \tag{52a}$$

where the leading term of (16) was considered by setting $n = 0$, $a_0(\sigma_m) = 1$, and $h(\xi) \sim o(\xi^4)$ in (48c). Using (20c–f), this expression tends to zero for $m = 1, 2, 3$ or $\sigma_m = 1, 0, -1$, but to a finite value for $m = 4$ or $\sigma_m = -2$, so the solution H_4 must be excluded by setting $C_4 = 0$; the condition of zero transverse force (48b) leads to

$$IV: \quad \lim_{\xi\to 0} \frac{\lambda - 1}{L} \frac{d}{d\xi} \left[h(\xi) H_m''(\xi) \right] = -\frac{1}{L} \lim_{\xi\to 0} \frac{d}{d\xi} \left[h(\xi) \frac{d^2}{d\xi^2} \sum_{n=0}^{\infty} a_n(\sigma_m) \xi^{n+\sigma_m} \right]$$

$$\sim \lim_{\xi\to 0} \frac{d}{d\xi} \left[\xi^4 \left(\frac{d^2}{d\xi^2} \xi^{\sigma_m} \right) \right] = \lim_{\xi\to 0} \sigma_m(\sigma_m - 1)(\sigma_m + 2) \xi^{\sigma_m+1} = 0\,, \tag{52b}$$

where the leading term of (16) was considered as in (52a). Using (20c–f), this expression tends to zero for $\sigma_m = 1, 0$ corresponding to $m = 1, 2$, to a finite value for $\sigma_m = -1$ corresponding to $m = 3$, and to infinity for $\sigma_m = -2$ corresponding to $m = 4$, so the solutions H_3 and H_4 are excluded by setting $C_3 = 0$ and $C_4 = 0$; Thus, in the case of a delta wing (53a) the condition (51) is replaced by (53b,c),

$$\lambda = 0: \quad C_3 = 0 = C_4, \qquad \begin{bmatrix} H_1(1) & H_2(1) \\ H_1'(1) & H_2'(1) \end{bmatrix} \begin{bmatrix} C_1 \\ C_2 \end{bmatrix} = 0\,. \tag{53a-c}$$

There are at most two non-zero constants of integration $(C_1, C_2) \neq (0, 0)$, and since they cannot both vanish, the determinant in (53c) must vanish,

$$0 = H_1(1) H_2'(1) - H_2(1) H_1'(1) \equiv J(\Omega, 0) = 0\,, \;, \tag{54a,b}$$

that is the Wronskian $J(\Omega, \lambda)$ of $[H_1(\xi), H_2(\xi)]$ at $\xi = 1$, defined by (54a), specifies through its roots $\Omega_n(0)$ the natural frequencies $\Omega_n(\lambda)$ in the case $\lambda = 0$ (53a) of a delta wing.

5. Comparison with the corresponding rectangular wing planform

The particular case, distinct from the preceding, which is the simplest, is the rectangular wing ($\lambda = 1$), with the same mean chord and thickness,

$$\bar{c} = c(y) = \text{const}\,, \quad \bar{e} = e(y) = \text{const}\,, \tag{55a,b}$$

for which the mass per unit span and area moment of inertia are constant,

$$\overline{m} = \rho \bar{c} \bar{e} \,, \quad \bar{I} = \frac{1}{12} \bar{c} \bar{e}^3 \,. \tag{56a,b}$$

In this case, the equation of transverse vibrations (8) has constant coefficients,

$$-\overline{m} \frac{\partial^2 X}{\partial t^2} = E \bar{I} \frac{\partial^4 X}{\partial y^4} \,, \tag{57}$$

and in the case (10) of constant frequency ω, it leads to

$$\frac{d^4 F}{dy^4} - \frac{\omega^2 \overline{m}}{E \bar{I}} F = 0 \,. \tag{58}$$

The change of independent variable

$$s \equiv \frac{y}{L} \,, \quad F(y) \equiv Q(s) \,, \tag{59a, b}$$

which implies that $\frac{d}{dy} = \frac{1}{L} \frac{d}{ds}$ and $\frac{d^2}{dy^2} = \frac{1}{L^2} \frac{d^2}{ds^2}$, leads to

$$Q'''' - \overline{\Omega}^2 Q = 0 \,, \tag{60a}$$

where the dimensionless frequency,

$$\overline{\Omega} \equiv \omega L^2 \sqrt{\frac{\overline{m}}{E \bar{I}}} = \frac{\omega L^2}{\bar{e}} \sqrt{\frac{12 \rho}{E}} \,, \tag{60b}$$

replaces (14a), which is not valid for $\lambda = 1$; note that the change of variable (12a) also does not apply for $\lambda = 1$, and was replaced by (59a). Notice that this definition of dimensionless frequency (60b) is equivalent to (14b) since the rectangular wing has constant section properties from root to tip.

The case of the rectangular wing is the simplest because (60a) has elementary solutions,

$$\alpha \equiv \sqrt{\overline{\Omega}} : \quad Q(s) = B_1 \cos(\alpha s) + B_2 \sin(\alpha s) + B_3 \cosh(\alpha s) + B_4 \sinh(\alpha s) \,. \tag{61}$$

The boundary conditions of clamping at the root $y = 0$, $s = 0$ (47a,b) can be expressed as

$$I : \qquad X(0, t) = 0 \Rightarrow \; F(0) = 0 \Rightarrow \; Q(0) = B_1 + B_3 = 0 \,, \tag{62a}$$

$$II : \qquad \frac{\partial X(0, t)}{\partial y} = 0 \Rightarrow \; F'(0) = 0 \Rightarrow \; Q'(0) = \alpha (B_2 + B_4) = 0 \,, \tag{62b}$$

which leaves two out of four constants of integration independent,

$$Q(s) = B_1 [\cos(\alpha s) - \cosh(\alpha s)] + B_2 [\sin(\alpha s) - \sinh(\alpha s)] \,. \tag{63}$$

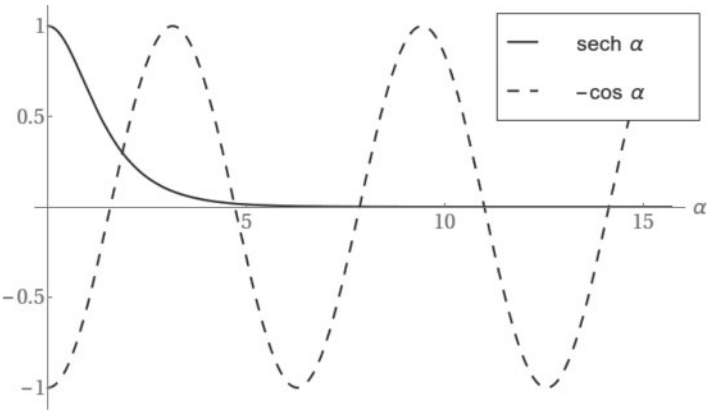

Fig. 4 Natural dimensionless frequencies $\overline{\Omega}_n = \alpha_n^2$ of rectangular wing determined by the intersections of $\operatorname{sech}\alpha$ and $-\cos\alpha$.

The boundary conditions at the tip $y = L$, $s = 1$ in (48a,b) lead to

$$III: \frac{\partial^2 X(L,t)}{\partial y^2} = 0 \quad \Rightarrow F''(1) = 0$$
$$\Rightarrow Q''(1) = -B_1(\cos\alpha + \cosh\alpha) - B_2(\sin\alpha + \sinh\alpha) = 0\,, \tag{64a}$$
$$IV: \frac{\partial^3 X(L,t)}{\partial y^3} = 0 \quad \Rightarrow F'''(1) = 0$$
$$\Rightarrow Q'''(1) = B_1(\sin\alpha - \sinh\alpha) - B_2(\cos\alpha + \cosh\alpha) = 0\,, \tag{64b}$$

form a linear homogeneous system, which has a non-trivial solution if the determinant of coefficients vanishes,

$$(B_1, B_2) \neq (0,0): \begin{vmatrix} \cos\alpha + \cosh\alpha & \sin\alpha + \sinh\alpha \\ \sinh\alpha - \sin\alpha & \cos\alpha + \cosh\alpha \end{vmatrix} = 2(1 + \cos\alpha\cosh\alpha) = 0\,. \tag{65a}$$

Thus the natural frequencies for the rectangular wing are the roots of

$$\lambda = 1: \quad \operatorname{sech}\left(\sqrt{\overline{\Omega}}\right) = -\cos\left(\sqrt{\overline{\Omega}}\right)\,, \tag{65b}$$

and are illustrated in Fig. 4.

The fundamental dimensionless frequency and higher harmonics, solution of (65b), were computed numerically using the software *Mathematica*® Version 11.0.1 and are summarized in Table 1. It yields for the dimensionless frequency of the fundamental mode $\alpha_1 = 1.8751$, leading to $\overline{\Omega}_1 = \alpha_1^2 = 3.5160$, which matches the well-known values of long, thin, cantilever beams (**12**) as expected.

Table 1 Fundamental dimensionless frequency and higher harmonics $\overline{\Omega}_n$ of a rectangular wing ($\lambda = 1$), where $\overline{\Omega}_n = \alpha_n^2 : f(\alpha_n) = \operatorname{sech}\alpha_n + \cos\alpha_n = 0$.

α_1	α_2	α_3	α_4	α_5	α_6	α_7	α_8
1.8751	4.6941	7.8548	10.996	14.137	17.279	20.420	23.562
$\overline{\Omega}_1$	$\overline{\Omega}_2$	$\overline{\Omega}_3$	$\overline{\Omega}_4$	$\overline{\Omega}_5$	$\overline{\Omega}_6$	$\overline{\Omega}_7$	$\overline{\Omega}_8$
3.5160	22.034	61.697	120.90	199.86	298.56	416.99	555.17

6. Natural frequencies for delta wing

The calculation of the fundamental frequency of bending oscillations is less simple for a non-rectangular wing because it involves the four non-elementary functions (39,40,44,45), of which only two are needed in the case (54b) of a delta wing (54a).

The first fundamental solution (39) has leading term ξ,

$$H_1(\xi) = 3!\xi\left[\frac{1}{3!} + \frac{(\Omega\xi)^2}{5!3!} + \frac{(\Omega\xi)^4}{7!5!} + O((\Omega\xi)^6)\right] = \xi + \frac{\Omega^2\xi^3}{120} + \frac{\Omega^4\xi^5}{100800} + O(\Omega^6\xi^7)\,. \tag{66}$$

The second fundamental solution (40) has leading term unity,

$$H_2(\xi) = 2!\left[\frac{1}{2!} + \frac{(\Omega\xi)^2}{4!2!} + \frac{(\Omega\xi)^4}{6!4!} + O((\Omega\xi)^6)\right] = 1 + \frac{\Omega^2\xi^2}{24} + \frac{\Omega^4\xi^4}{8640} + O(\Omega^6\xi^6)\,. \tag{67}$$

In the case of delta wing (53a)≡(68a), the other two fundamental solutions (44) and (45) do not appear (53b,c) in the general solution (21) that simplifies to (68b),

$$\lambda = 0: \qquad G(\xi) = C_1 H_1(\xi) + C_2 H_2(\xi)\,. \tag{68a,b}$$

The condition (54b) specifying the natural frequencies for the delta wing also involve the derivatives of the fundamental solutions (39) and (40),

$$\begin{aligned} H_1'(\xi) &= 3!\sum_{n=0}^{\infty}\frac{(\Omega\xi)^{2n}}{(2n+3)!(2n)!} \\ &= 3!\left[\frac{1}{3!} + \frac{(\Omega\xi)^2}{5!2!} + \frac{(\Omega\xi)^4}{7!4!} + O((\Omega\xi)^6)\right] = 1 + \frac{\Omega^2\xi^2}{40} + \frac{\Omega^4\xi^4}{20160} + O(\Omega^6\xi^6)\,, \end{aligned} \tag{69}$$

$$\begin{aligned} H_2'(\xi) &= 2!\Omega\sum_{m=1}^{\infty}\frac{(\Omega\xi)^{2m-1}}{(2m+2)!(2m-1)!} = 2!\Omega\sum_{n=0}^{\infty}\frac{(\Omega\xi)^{2n+1}}{(2n+4)!(2n+1)!} \\ &= 2!\Omega\left[\frac{\Omega\xi}{4!} + \frac{(\Omega\xi)^3}{6!3!} + \frac{(\Omega\xi)^5}{8!5!} + O((\Omega\xi)^7)\right] = \frac{\Omega^2\xi}{12} + \frac{\Omega^4\xi^3}{2160} + \frac{\Omega^6\xi^5}{2419200} + O(\Omega^8\xi^7)\,. \end{aligned} \tag{70}$$

The condition (54b) that specifies the natural frequencies of the delta wing (54a) can then be used.

Table 2 Calculation of the fundamental dimensionless frequency and higher harmonics Ω_n of a delta wing ($\lambda = 0$), to successively higher orders in $\Omega^{(2N)}$.

N	$\pm\Omega_1^{(N)}$	$\pm\Omega_2^{(N)}$	$\pm\Omega_3^{(N)}$	$\pm\Omega_4^{(N)}$	$\pm\Omega_5^{(N)}$	$\pm\Omega_6^{(N)}$	$\pm\Omega_7^{(N)}$	$\pm\Omega_8^{(N)}$
5	8.7193	21.066	—	—	—	—	—	—
10	8.7193	21.146	38.454	60.673	—	—	—	—
15	8.7193	21.146	38.454	60.680	87.834	119.92	—	—
20	8.7193	21.146	38.454	60.680	87.834	119.92	156.94	198.89
⋮	⋮	⋮	⋮	⋮	⋮	⋮	⋮	⋮
50	8.7193	21.146	38.454	60.680	87.834	119.92	156.94	198.89

The simplification of condition (54b) is detailed in Appendix B, and its numerical evaluation using *Mathematica*® for the fundamental and higher order approximations are included in Table 2. It yields for the dimensionless fundamental frequency for the delta wing $\Omega_1(0) = 8.7193$, which is higher than for the rectangular wing, because the delta wing is stiffer, that is, it has a larger fraction of the mass near the root. Notice that for the delta wing ($\lambda = 0$), (14c) yields $\widetilde{\Omega}(0) = \Omega(0)$.

7. Natural frequencies for general tapered wings

For the general tapered wing case, the evaluation of the natural bending frequencies implies the solution of a four by four determinant (51). The proper boundary conditions were applied to the four independent solutions (39, 40, 44, 45) and the first five roots of (51) were computed numerically using *Mathematica*® for different values of wing taper ratio. Based on the convergence observed in the delta wing case, only the first 50 terms in the series were used ($n_{\max} = 50$). These results are summarized in Table 3, where for completeness the rectangular wing case was added in the last column from Table 1. It can be observed a near perfect agreement with the available corresponding analytic and numerical results included in the literature (**12**). The entries *nc* represent non-converged numerical solutions, that resulted from the poor conditioning of the system (51) as $\lambda \to 1$.

As expected, the dimensionless frequency $\Omega_n(\lambda)$, expressed in (14a), is a monotonically increasing function in λ, bounded below but unbounded above,

$$0 \le \lambda < 1: \quad \Omega_n(0) \le \Omega_n(\lambda) < \infty\,. \tag{71}$$

In contrast, the usual definition of the dimensionless frequency $\widetilde{\Omega}_n(\lambda)$ (14b) exhibits a different behavior, as graphically observed in Fig. 5. The fundamental frequency $\widetilde{\Omega}_1(\lambda)$ is a monotonically decreasing function of taper ratio λ, differently from other modes which either exhibit a minimum as a function of λ ($\widetilde{\Omega}_2(\lambda)$ and $\widetilde{\Omega}_3(\lambda)$, respectively modes 2 and 3), or are monotonically increasing functions of λ ($\widetilde{\Omega}_4(\lambda)$ and $\widetilde{\Omega}_5(\lambda)$, respectively modes 4 and 5).

The results in Table 3 can be converted from dimensionless Ω to dimensional ω frequency using (14a) and (60b). For illustration, considering only the fundamental frequency, yields

Table 3 Fundamental dimensionless frequency as function of taper ratio λ.

λ	0.0	0.1	0.2	0.3	0.4	0.5	0.6	0.7	0.8	0.9	1.0
$\Omega_1(\lambda)$	8.7193	8.8949	9.6819	11.243	13.914	18.501	26.992	45.188	93.304	367.62	
$\widetilde{\Omega}_1(\lambda)$	8.7193	7.2049	6.1964	5.5093	5.0090	4.6252	4.3188	4.0669	3.8522	3.6762	3.5160
$\Omega_2(\lambda)$	21.145	23.062	28.727	38.043	52.958	78.186	123.47	227.56	527.50	2150.7	
$\widetilde{\Omega}_2(\lambda)$	21.145	18.680	18.386	18.641	19.065	19.547	19.757	20.481	21.100	21.507	22.034
$\Omega_3(\lambda)$	38.454	45.832	62.240	87.368	126.52	193.67	319.48	598.12	1410.7	*nc*	
$\widetilde{\Omega}_3(\lambda)$	38.454	37.124	39.834	42.810	45.547	48.418	51.116	53.831	56.426	*nc*	61.697
$\Omega_4(\lambda)$	60.680	78.401	111.32	159.47	237.12	367.36	626.84	1155.3	*nc*	*nc*	
$\widetilde{\Omega}_4(\lambda)$	60.680	63.505	71.242	78.141	85.362	91.839	100.29	103.98	*nc*	*nc*	120.90
$\Omega_5(\lambda)$	87.834	121.19	176.12	255.81	383.38	598.37	*nc*	*nc*	*nc*	*nc*	
$\widetilde{\Omega}_5(\lambda)$	87.834	98.166	112.72	125.35	138.02	149.59	*nc*	*nc*	*nc*	*nc*	199.86

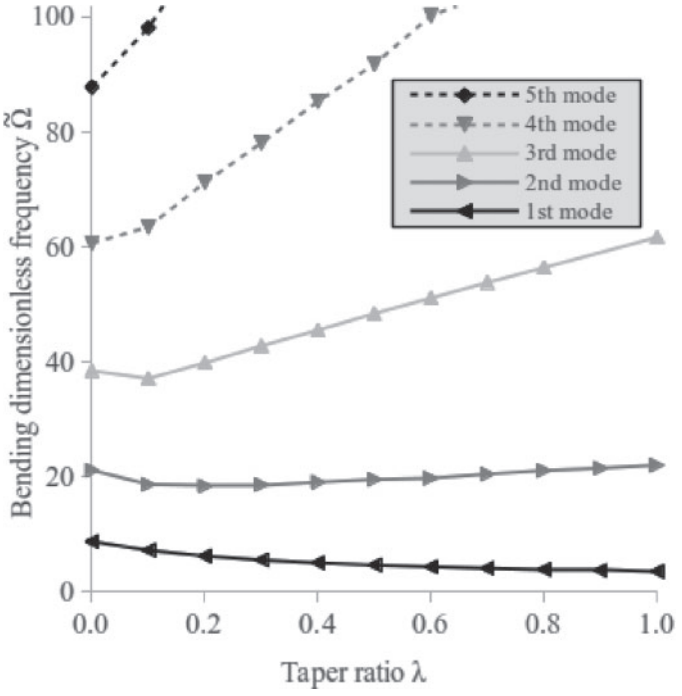

Fig. 5 Natural vibration dimensionless frequencies $\widetilde{\Omega}_n(\lambda)$, corresponding to the first five bending modes n, for general tapered wings with taper ratios λ ranging from 0 (delta wing) to 1 (rectangular wing).

$$\lambda = 1: \quad \overline{\omega}_1 = \frac{\overline{\Omega}_1 \, \bar{e}}{L^2} \sqrt{\frac{E}{12\rho}}$$

$$= \frac{3.5160 \times 0.1}{6^2} \sqrt{\frac{70 \times 10^9}{12 \times 2700}} = 14.356 \text{ rad s}^{-1} = 2.2848 \text{ Hz}, \tag{72a}$$

$$\lambda = 0: \quad \omega_1 = \frac{\Omega_1(0) \, \bar{e}}{L^2} \sqrt{\frac{E}{3\rho}}$$

$$= \frac{8.7193 \times 0.1}{6^2} \sqrt{\frac{70 \times 10^9}{3 \times 2700}} = 71.201 \text{ rad s}^{-1} = 11.332 \text{ Hz}, \tag{72b}$$

$$0 < \lambda < 1: \quad \omega_1 = \frac{\Omega_1(\lambda) \, \bar{e}}{L^2} \sqrt{\frac{E}{3\rho}} \frac{(\lambda - 1)^2}{\lambda + 1}, \tag{72c}$$

where the values (72a) and (72b) were calculated for an aluminium wing with Young's modulus $E = 70$ GPa, density $\rho = 2700 \text{ kg m}^{-3}$, semi-span $L = 6$ m and mean thickness $\bar{e} = 0.1$ m. The fundamental frequency varies most between the delta and rectangular wing,

$$\frac{\Omega_1}{\overline{\Omega}_1} = \frac{\Omega_1(0)}{\Omega_1(1)} = 2.48, \qquad \frac{\omega_1}{\overline{\omega}_1} = 2\frac{\Omega_1}{\overline{\Omega}_1} = 4.96. \tag{73a,b}$$

Even though the two definitions of dimensionless frequencies (14a) and (60b) are not continuous at $\lambda = 1$, when converted to dimensional frequency, it becomes monotonically decreasing and continuous in λ, bounded below and above, as physically expected, and as observed considering the usual definition $\widetilde{\Omega}$ (14b). For the particular example above, it can be seen that the fundamental natural bending frequency of a tapered wing lies between the two extreme conditions, the delta (upper bound) and the rectangular (lower bound) wings,

$$0 \leq \lambda \leq 1: \quad 71.201 \text{ rad s}^{-1} = \omega_1(0) \geq \omega_1(\lambda) \geq \overline{\omega}_1 = \omega_1(1) = 14.356 \text{ rad s}^{-1}. \tag{74}$$

and for a wing with intermediate taper ratio,

$$\lambda = 1/2: \ \omega = \frac{\Omega_1(1/2) \, \bar{e}}{L^2} \sqrt{\frac{E}{108\rho}}$$

$$= \frac{18.500 \times 0.1}{6^2} \sqrt{\frac{70 \times 10^9}{108 \times 2700}} = 25.178 \text{ rad s}^{-1} = 4.0072 \text{ Hz}, \tag{75}$$

lies in the range (74).

8. Comparison with numerical models

To compare analytical solutions with numerical models, a total of eleven cases ranging from $\lambda = 0$ to $\lambda = 1$ in 0.1 increments were modelled using a finite element model created in *ANSYS*® Version 2019, where the material and geometric properties matched those used in the example in section 7.

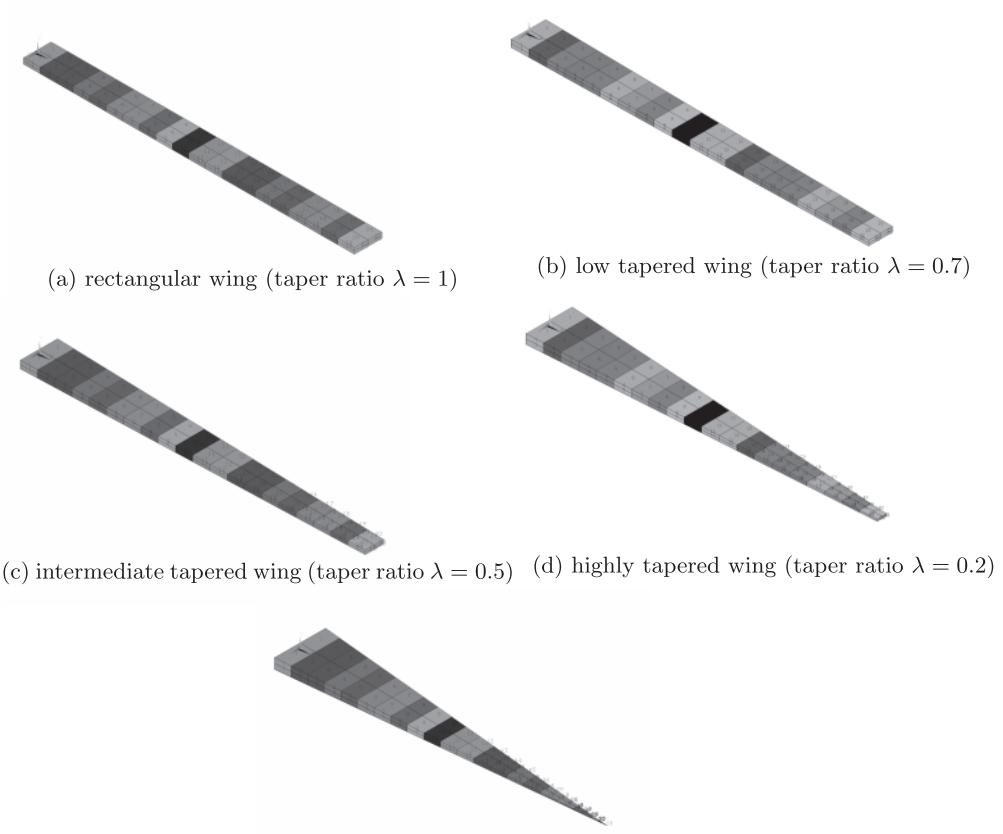

Fig. 6 Perspective view of some of the *ANSYS*® models using *beam188* element type. Modal analyses performed with meshes ranging from 10 to 320 elements (20 element mesh shown), assuming clamped root (upper left end)—free tip (bottom right end) boundary conditions.

Emphasis is given to three cases: the two extreme cases of tapered wing spar geometries, a rectangular ($\lambda = 1$) and a delta beam ($\lambda = 0$), replicating the conditions used in (72a) and (72b), respectively, and an intermediate tapered beam ($\lambda = 1/2$) replicating the conditions in (75), as illustrated in Fig. 6(a), (e) and (c), respectively.

Since the analysis was restricted to unswept tapered wings, where all cross-sections are perpendicular to the beam axis, a 1D beam element was found appropriate for the numerical simulation since it mimics the standard beam theory used in (8). The linear finite strain beam *beam188* element type was used due to its capability to model both constant (uniform) and varying (tapered) cross-sections, required for the rectangular and tapered wings, respectively, of which the delta wing is a particular case of the latter.

The beam element has two nodes and it was set as a linear element (quadratic or cubic was also possible) to suit the linear case study. Since the degrees of freedom at each beam element node include

(a) front view (b) top view

Fig. 7 Linearly tapered beam, both in thickness (height) and chord (width), modelled in *ANSYS*® models using *beam188* element type, assuming clamped root (left end) –free tip (right end) boundary conditions. Illustration of intermediate tapered wing ($\lambda = 0.5$) with 20 element mesh.

Table 4 First 8 natural frequencies of the rectangular wing using *ANSYS*®.

f [Hz]	No. of elements						$\overline{\Omega}_n$
Mode	10	20	40	80	160	320	
1*	2.2862	2.2847	2.2844	2.2843	2.2843	2.2843	3.5153
2	11.370	11.363	11.361	11.361	11.361	11.361	17.483
3*	14.611	14.375	14.316	14.301	14.297	14.297	22.001
4*	42.580	40.586	40.104	39.984	39.954	39.946	61.472
5	48.640	48.599	48.590	48.587	48.587	48.586	74.768
6	70.412	69.322	69.052	68.984	68.967	68.963	106.13
7*	88.883	80.597	78.663	78.188	78.070	78.041	120.10
8*	147.11	135.66	130.22	128.91	128.58	128.50	197.75

translation and rotation in all directions, the modal analyses capture all vibration modes: bending, torsion and axial. The modal analyses covered only the first eight vibration modes, of which it was concluded by observation of the modes shapes that five correspond to transverse bending. It should be noted that, despite the nonlinear finite strain beam model capability, the modal analysis conducted in *ANSYS*® is linear, being the stiffness matrix and mass matrix computed for the undeformed beam shape, so the same behaviour and results as those of the analytical analyses shown in Fig. 5 were to be expected.

An increasing number of finite-elements was used until a good convergence of the vibration frequencies are obtained for the bending modes. This implied beam meshing ranging from 10 to 320 elements. The spanwise linear distribution of chord (beam width) (2) and thickness (beam height) (3) can be observed in Fig. 7, where the intermediate taper beam *ANSYS*® model is shown as illustration.

Figure 6(a) shows the rectangular beam model ($\lambda = 1$) and Table 4 summarizes the results for different number of finite elements. The dimensional frequency corresponding to the most refined discretization has been made non-dimensional using expression (60b). By observing the mode shapes in *ANSYS*®, it was possible to identify the (vertical) transverse bending modes, which correspond to modes 1, 3, 4, 7 and 8 and are marked with asterisk in Table 4. The modes 2 and 6 correspond to horizontal bending, and mode 5 to torsion. The solution for the first mode, corresponding to the fundamental transverse bending frequency, converges to the expected value (72a). The same can be said of the higher transverse bending modes that converge to the analytical values in Table 1.

Table 5 First 8 natural frequencies of the tapered wing using *ANSYS*®.

f [Hz]	No. of elements						Ω_n
Mode	10	20	40	80	160	320	
1*	3.9939	4.0029	4.0051	4.0057	4.0058	4.0059	18.494
2*	17.171	16.976	16.925	16.913	16.910	16.909	78.063
3	19.794	19.838	19.849	19.852	19.852	19.852	91.650
4*	44.341	42.533	42.080	41.967	41.939	41.932	193.59
5	78.136	78.143	78.144	78.145	78.145	78.145	360.77
6*	82.594	81.455	79.611	79.154	79.040	79.012	364.77
7	89.061	81.691	81.460	81.401	81.837	81.383	375.72
8*	157.42	134.95	129.74	128.47	128.15	128.07	591.26

Figure 6(c) shows the tapered beam model ($\lambda = 1/2$) and Table 5 summarizes the results for different number of finite elements. The dimensional frequency corresponding to the most refined discretization has been made non-dimensional using expression (14a). In this case, the mode shapes indicated that the (vertical) transverse bending modes correspond to modes 1, 2, 4, 6 and 8, marked with asterisk in Table 5. The modes 3 and 7 correspond to horizontal bending, and mode 5 to torsion. The five transverse bending modes are illustrated in Fig. 8. Again, the solution for the fundamental transverse bending frequency converges to the expected value (75). The second to fifth bending modes also converge to the analytical values in the corresponding taper ratio column found in Table 3.

Figure 6(e) shows the delta beam model ($\lambda = 0$), and Table 6 summarizes the results for different number of finite elements. The dimensional frequency corresponding to the most refined discretization has been made non-dimensional using expression (14a). The (vertical) transverse bending correspond to modes 1, 2, 3, 5 and 6, which are marked with asterisk in Table 6, modes 4 and 7 correspond to horizontal bending, and mode 8 to torsion. Once again, the solution for the fundamental transverse bending frequency converges to the expected value (72b). The same can be said of the higher transverse bending modes that converge to the numerical evaluations of the analytical expression in Table 2.

Compiling the 11 cases run for the complete taper ratio range, a graphical comparison between transverse bending frequencies obtained by both the analytical approach outlined in this paper and by the numerical simulations using *ANSYS*® is shown in Fig. 9 for the first three bending modes of vibration. The analytical values obtained for the dimensionless frequency were converted to dimensional using (14a) and (60b) for the tapered ($0 \leq \lambda < 1$) and rectangular ($\lambda = 1$) beams, respectively.

In Fig. 9, it can be observed an excellent agreement between these two fundamentally distinct analyses, with a registered maximum difference of 0.1%, 1.3% and 0.4% for the first, second and third bending modes, respectively. Given the proven validation of the numerical model used in the finite-element software, this result proves the correct analytical development presented in this article.

It should be noted that, had a swept wing been modelled (either sweptback or sweptforward), these results would not apply since the boundary cross-sections would not be perpendicular to the beam axis, as assumed in the beam equation (8) and the applied clamped wing root and free wing tip boundary conditions, respectively through (47) and (48).

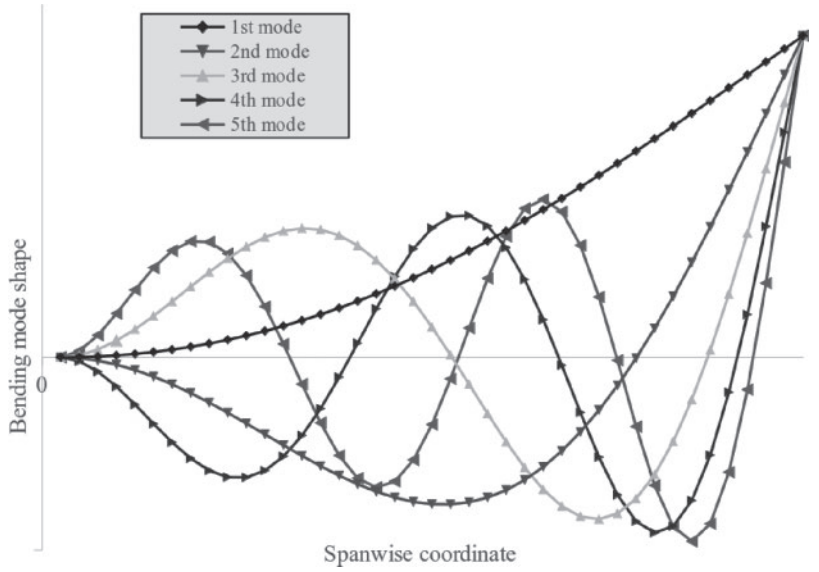

Fig. 8 Bending shape modes for mid-tapered wing ($\lambda = 0.5$) using *ANSYS*®. The five bending modes correspond to the modes numbers with asterisk in Table 5.

Table 6 First 8 natural frequencies of the delta wing obtained using *ANSYS*®.

f [Hz]	No. of elements						Ω_n
Mode	10	20	40	80	160	320	
1*	11.108	11.270	11.307	11.316	11.319	11.319	8.7093
2*	25.160	27.096	27.356	27.406	27.417	27.420	21.098
3*	38.631	47.572	49.511	49.739	49.783	49.793	38.313
4	54.179	54.924	55.095	55.137	55.147	55.150	42.435
5*	63.546	68.039	77.227	78.271	78.407	78.435	60.351
6*	107.97	94.727	108.17	112.81	113.23	113.30	87.178
7	121.32	129.11	130.14	130.34	130.39	130.40	100.34
8	138.56	136.27	138.96	138.98	138.98	138.99	106.94

9. Discussion and conclusions

The natural bending frequency of a tapered wing was derived using the governing differential equation for the unsteady deflection of a beam. The frequencies were obtained by casting the problem in the form of an eigenvalue problem, which translated into a root finding problem, $H(\Omega, \lambda) = 0$, once the proper expressions were derived for the tapered wing.

As expected, for wings with the same span and mean chord (and thus area) and material, the fundamental natural bending frequency is higher for a delta planform, when compared to a rectangular

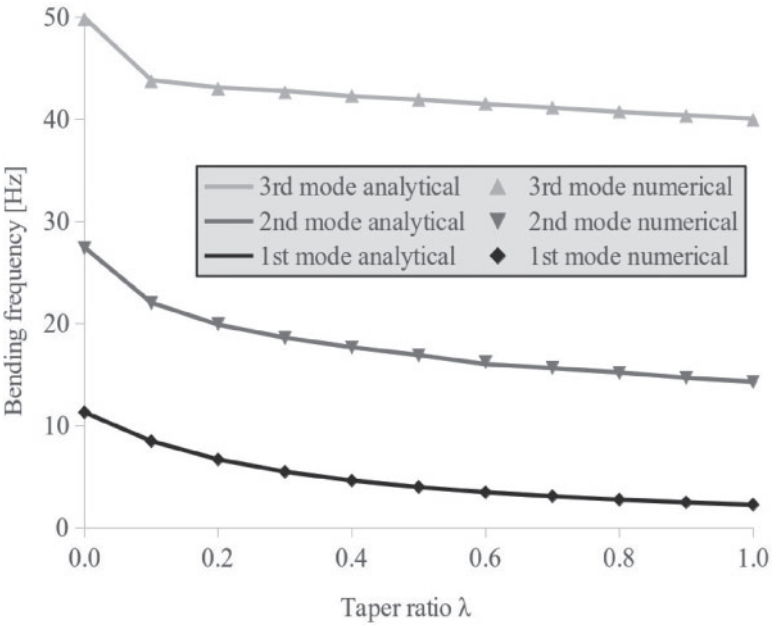

Fig. 9 Validation of numerical simulations with the analytical solutions. Overlap of first three bending frequencies obtained from both approaches show a visually perfect match regardless of the taper ratio wing configuration.

planform, by a factor of 4.96. A tapered planform exhibits a frequency that lies within these two cases.

The analytical theory was compared with a widely used commercial finite element code in the three cases of: (a) rectangular (i) or delta (ii) wing; (b) intermediate case (iii) of tapered form. It was demonstrated that the analytical theory presented closely agrees with the *ANSYS*® finite element code as concerns the natural frequencies of the bending modes for either (i) the rectangular wing, (ii) the delta wing and (iii) any intermediate tapered wing. The very small discrepancies can be attributed both to the numerical errors, related to the finite-element theory and the computation itself and to the finite number of the terms in (39, 40, 44, 45) considered when analytically solving (51).

In conclusion, the analytical theory developed in this article covers all solutions of the wing bending equation, namely: (a) the regular solutions for (i) rectangular and (ii) delta wings; (b) the singular solutions for the intermediate cases of (iii) tapered wings.

The elastic vibration equation (8) applies to a wing with arbitrary planform and thickness distributions along the span. The detailed solution in the case of equation (9) applies for: (i) chord varying linearly along the span; (ii) constant thickness-to-chord ratio, implying that the thickness also varies linearly along the span. The simplest case of (i) chord varying linearly along the span is a wing planform with straight leading and trailing edges. The general method presented applies to arbitrary wing planforms and spanwise thickness distributions, with corresponding modification of the details of the analysis. In the examples chosen, the beam was far removed from a prismatic beam

with square cross-section, since the chord is usually much larger than the thickness by more than an order of magnitude.

Acknowledgements

This work was supported by Fundação para a Ciência e a Tecnologia (FCT) through IDMEC (Institute of Mechanical Engineering), under LAETA, project UID/EMS/50022/2020.

References

1. A. Cazzani, L. Rosati and P. Ruge, The contribution of Gustav R. Kirchhoff to the dynamics of tapered beams, *Z. Angew. Math. Mech.* **97** (2017) 1174–1203.
2. S. Naguleswaran, Vibration of an Euler–Bernoulli beam of constant depth and with linearly varying breadth, *J. Sound Vib.* **153** (1992) 509–522.
3. G. Kirchhoff. *Uber die Transversalschwingungen eines Stabes von veränderlichem Querschnitt*, pages 815–828. Monatsbericht der königlichen preussischen Akademie der Wissenschaften zu Berlin aus dem Jahre 1979, 1880.
4. D. Wrinch, On the lateral vibrations of bars of conical type, *Proc. R. Soc. Lond. A* **101** (1922) 493–508.
5. A. Ono, Lateral vibrations of tapered bars, *Journal of the Society of Mechanical Engineers in Japan* **28** (1925) 429–441.
6. H. D. Conway, E. C. H. Becker and J. F. Dubil, Vibration frequencies of tapered bars and circular plates, *J. Appl. Mech.* **31** (1964) 329–331.
7. J. H. Lau, Vibration frequencies of tapered bars with end mass, *J. Appl. Mech.* **51** (1984) 179–181.
8. J. H. Gaines and E. Volterra, Transverse vibrations of cantilever bars of variable cross section, *J. Acoust. Soc. Am.* **39** (1966) 674–679.
9. H.-C. Wang, Generalized hypergeometric function solutions on the transverse vibration of a class of nonuniform beams, *J. Appl. Mech.* **34** (1967) 702–708.
10. H.-C. Wang and W. J. Worley, Tables of natural frequencies and nodes for transverse vibration of tapered beams, NASA Contractor Report CR-443, University of Illinois, (1966).
11. K. Sato, Transverse vibrations of linearly tapered beams with ends restrained elastically against rotation subjected to axial force, *Int. J. Mech. Sci.* **22** (1980) 109–115.
12. B. Downs, Transverse vibrations of cantilever beams having unequal breadth and depth tapers, *J. Appl. Mech.* **44** (1977) 737–742.
13. R. S. Chen, Evaluation of natural vibration frequency and buckling loading of bending bar by searching zeros of a target function, *Commun. Numer. Methods Eng.* **13** (1997)695–704.
14. M. Amabili and R. Garziera, A technique for the systematic choice of admissible functions in the Rayleigh–Ritz method, *J. Sound Vib.* **224** (1999) 519–539.
15. D. Zhou and Y. K. Cheung, The free vibration of a type of tapered beams. *Comput. Method Appl. M.*, **188** (2000) 203–216.
16. M. Bayat, I. Pakar and M. Bayat, Analytical study on the vibration frequencies of tapered beams, *Lat. Am. J. Solids Struct.*, **8** (2011) 149–162.
17. C. Y. Wang, Vibration of a tapered cantilever of constant thickness and linearly tapered width, *Arch. Appl. Mech.* **83** (2013) 171–176.

18. C.-S. Chang and D. H. Hodges, Parametric studies on ground vibration test modeling for highly flexible aircraft, *J. Aircraft* **44** (2007) 2049–2059.
19. J. R. Banerjee, Modal analysis of sailplane and transport aircraft wings using the dynamic stiffness method, *J. Phys. Conf. Ser.* **721** (2016).
20. W. Su and C. E. S. Cesnik, Dynamic response of highly flexible flying wings, *AIAA J.*, **49** (2011) 324–339.
21. F. Saltari, C. Riso, G. De Matteis and F. Mastroddi, Finite-element-based modeling for flight dynamics and aeroelasticity of flexible aircraft, *J. Aircraft* **54** (2017) 2350–2366.
22. A. V. Balakrishnan and K. W. Iliff, Continuum aeroelastic model for inviscid subsonic bending-torsion wing flutter, *J. Aerosp. Eng.* **20** (2007) 152–164.
23. X. Changchuan, Y. Lan, L. Yi and Y. Chao, Stability of very flexible aircraft with coupled nonlinear aeroelasticity and flight dynamics, *J. Aircraft* **55** (2018) 862–874.
24. X. Rui, L. K. Abbas, F. Yang, G. Wang, H. Yu and Y. Wang, Flapwise vibration computations of coupled helicopter rotor/fuselage: application of multibody system dynamics, *AIAA J.* **56** (2018) 818–835.
25. D. Storti and Y. Aboelnaga, Bending vibrations of a class of rotating beams with hypergeometric solutions, *J. Appl. Mech.*, **54** (1987) 311–314.
26. H. H. Yoo and S. H. Shin, Vibration analysis of rotating cantilever beams, *J. Sound Vib.*, **212** (1998) 807–828.
27. N. M. Auciello and M. J. Maurizi, On the natural vibrations of tapered beams with attached inertia elements, *J. Sound Vib.* **199** (1997) 522–530.
28. T. Kant and K. Swaminathan, Analytical solutions for free vibration of laminated composite and sandwich plates based on a higher-order refined theory, *Compos. Struct.* **53** (2001) 73–85.
29. J. Fernandez-Saez and C. Navarro, Fundamental frequency of cracked beams in bending in vibrations: an analytical approach, *J. Sound Vib.* **256** (2002) 17–31.
30. J. Woo, S. A. Meguid and L. S. Ong, Nonlinear free vibration behavior of functionally graded plates, *J. Sound Vib.* **289** (2006) 595–611.
31. L.-L. Ke, J. Yang and S. Kitipornchai, An analytical study on the nonlinear vibration of functionally graded beams, *Meccanica* **45** (2010) 743–752.
32. P. Lu, H. P. Lee, C. Lu and P. Q. Zhang, Application of nonlocal beam models for carbon nanotubes, *Int. J. Solids Struct.* **44** (2007) 5289–5300.
33. M. Strozzi, L. I. Manevitch, F. Pellicano, V. V. Smirnov and D. S. Shepelev, Low-frequency linear vibrations of single-walled carbon nanotubes: analytical and numerical models, *J. Sound Vib.* **333** (2014) 2936–2957.
34. I. Mirsky, Axisymmetric vibrations of orthotopic cylinders, *J. Acoust. Soc. Am.* **36**(1964) 2106–2112.
35. K. P. Soldatos, Review of three dimensional dynamic analyses of circular cylinders and cylindrical sheels, *Appl. Mech. Rev.* **47** (1994) 501–516.
36. A. L. Shuvalov, The Frobenius power series solution for cylindrically anisotropic radially inhomogeneous elastic materials, *Q. J. Mech. Appl. Math.* **56** (2003) 327–345.
37. S. Y. Lee and J. J. Sheu, Free vibrations of a rotating inclined beam, *J. Appl. Mech.* **74** (2007) 406–414.
38. N. Tutuncu, Stresses in thick-walled FGM cylinders with exponentially-varying properties, *Eng. Struct.* **29** (2007) 2032–2035.
39. M. Gharibi, M. Z. Nejad and A. Hadi, Elastic analysis of functionally graded rotating thick cylindrical pressure vessels with exponentially-varying properties using power series method

of Frobenius, *J. Comp. Appl. Mech.* **48** (2017) 89–98.
40. D. Adair and M. Jaeger, A power series solution for rotating nonuniform Euler–Bernoulli cantilever beams, *J. Vib. Control* **24** (2018) 3855–3864.
41. L. M. B. C. Campos. *Ordinary Differential Equations with Applications to Trajectories and Vibrations* (Taylor & Francis, Oxfordshire, UK 2019).
42. M. Abramowitz and I. A. Stegun. *Handbook of Mathematical Functions*, revised edn. (Dover Publications, New York, USA 1965).

APPENDIX

A. Comparison of different tapered beams

The transverse vibration of an Euler–Bernoulli beam satisfies the equation of bending waves (8), here rewritten for constant Young's modulus as

$$\frac{\partial^2}{\partial y^2}\left[EI(y)\frac{\partial^2 X(y,t)}{\partial y^2}\right] = -m(y)\frac{\partial^2 X(y,t)}{\partial t^2}\,. \tag{A.1}$$

Limiting to the analysis of the vibration modes using (10), yields the ordinary differential equation

$$\frac{d^2}{dy^2}\left[I(y)\frac{d^2F(y)}{dy^2}\right] = \frac{\omega^2 m(y)}{E}F(y)\,. \tag{A.2}$$

Following Kirchhoff's work (**3**), it is assumed a change in the cross-section given by

$$x \sim y^{\mu}\,, \quad z \sim y^{\nu}\,, \tag{A.3a, b}$$

where μ and ν are constants which respectively define the change in the height (transverse) and width directions (see Fig. 3). The moment of inertia and the mass per unit length can then be expressed, respectively, as

$$I(y) = I_1\left(\frac{y}{L}\right)^{3\mu+\nu}\,, \quad m(y) = m_1\left(\frac{y}{L}\right)^{\mu+\nu}\,, \tag{A.4a, b}$$

where I_1 and m_1 are the moment of inertia and the mass per unit length at the tip of the beam ($y = L$). Substituting (A.4) in (A.2), making the change of independent variable $\zeta \equiv y/L$, and using $F(y) \equiv K(\zeta)$ leads to the ordinary differential equation (ODE)

$$\frac{d^2}{d\zeta^2}\left[\zeta^{3\mu+\nu}\frac{d^2K(\zeta)}{d\zeta^2}\right] = \frac{\omega^2 m_1 L^4}{EI_1}\,\zeta^{\mu+\nu}\,K(\zeta)\,. \tag{A.5}$$

The analytical study of the transversal vibration of a pyramidal, linearly tapered, Euler–Bernoulli beam has already been tackled for different possible cases based on the ODE (A.5).

Assuming constant height ($\mu = 0$) and linearly varying width ($\nu = 1$) (see Fig. A.1(a)), the moment of inertia is a linear function ($I(\zeta) \sim \zeta$) and the mass per unit span is also a linear function ($m(\zeta) \sim \zeta$), and the ODE (A.5) is written as

$$\frac{d^2}{d\zeta^2}\left[\zeta\frac{d^2K(\zeta)}{d\zeta^2}\right] = \frac{\omega^2 m_1 L^4}{EI_1}\,\zeta\,K(\zeta)\,, \tag{A.6}$$

which was presented as (9) in (**2**) and solved for different boundary conditions (clamped, pinned, sliding and free) for both complete and truncated beams.

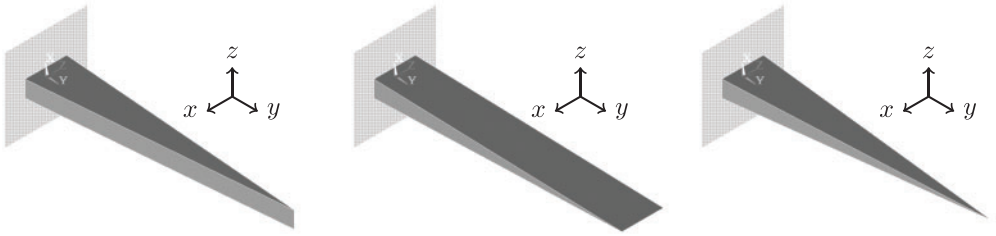

(a) linear width ($\mu = 0\,,\ \nu = 1$)

(b) linear height ($\mu = 1\,,\ \nu = 0$)

(c) linear width and height ($\mu = 1\,,\ \nu = 1$)

Fig. A.1 Different cases of a sharp tapered beam with linearly varying cross section

In contrast, assuming linearly varying height ($\mu = 1$) and constant width ($\nu = 0$) (see Fig. A.1(b)), the moment of inertia is now a cubic function ($I(\zeta) \sim \zeta^3$) and the mass per unit span is still a linear function ($m(\zeta) \sim \zeta$), so the ODE (A.5) becomes

$$\frac{d^2}{d\zeta^2}\left[\zeta^3 \frac{d^2K(\zeta)}{d\zeta^2}\right] = \frac{\omega^2 m_1 L^4}{EI_1}\,\zeta\,K(\zeta)\,, \tag{A.7}$$

which was expressed as Equation (B.19) in (**1**) and solved for the clamped-free boundary conditions following Kirchhoff's work (**3**).

The present article handles the combination of both linearly varying height and width ($\mu = 1 = \nu$) (see Fig. A.1(c)), maintaining a constant height-to-width ratio for a rectangular cross-section. Such beam taper implies that the moment of inertia is a quartic function ($I(\zeta) \sim \zeta^4$) and the mass per unit span is a quadratic function ($m(\zeta) \sim \zeta^2$), thus yielding

$$\frac{d^2}{d\zeta^2}\left[\zeta^4 \frac{d^2K(\zeta)}{d\zeta^2}\right] = \frac{\omega^2 m_1 L^4}{EI_1}\,\zeta\,K(\zeta)\,. \tag{A.8}$$

This equation is equivalent to (13) in which the change of variable (12a,b) is used.

Notice that, even though Fig. A.1 illustrates sharp end beams, Equations (A.6), (A.7) and (A.8) also apply to truncated beams by properly handling the tip boundary conditions.

B. Calculation of eigenvalues for the delta wing

Substituting (66,67,69,70) in the condition (54b) specifying the eigenvalues leads to the equality of the products of two series,

$$\sum_{n=0}^{\infty} \frac{(\Omega)^{2n}}{(2n+3)!(2n+1)!} \sum_{m=0}^{\infty} \frac{(\Omega)^{2m+1}}{(2m+4)!(2m+1)!} = \sum_{n=0}^{\infty} \frac{(\Omega)^{2n}}{(2n+2)!(2n)!} \sum_{m=0}^{\infty} \frac{(\Omega)^{2m}}{(2m+3)!(2m)!}\,. \tag{B.9}$$

Using the Cauchy rule for the summation of double series by diagonals,

$$\left(\sum_{n=0}^{\infty} b_n\right)\left(\sum_{m=0}^{\infty} c_m\right) = \sum_{n=0}^{\infty}\sum_{m=0}^{n} b_m c_{n-m}\,, \tag{B.10}$$

leads to the single series

$$0 = \sum_{n=0}^{\infty} d_n \Omega^{2n} \equiv P_{\infty}(\Omega^2) = \Pi_{k=1}^{\infty}\left(\Omega^2 - \Omega_k^2\right)\,, \tag{B.11}$$

with coefficients

$$d_n \equiv \sum_{m=0}^{n}\left\{\frac{1}{(2m+1)!(2m+3)!(2n-2m+1)!(2n-2m+4)!} - \frac{1}{(2m)!(2m+2)!(2n-2m)!(2n-2m+3)!}\right\}. \tag{B.12}$$

The roots of (B.11) are $\pm\Omega_k$, where Ω_k are the natural frequencies.

The successive approximations to the eigenvalues can be obtained by considering the series (B.11) truncated after $N+1$ terms, which is a polynomial of degree N in Ω^2,

$$P_N(\Omega^2) \equiv \sum_{n=0}^{N} d_n \Omega^{2n} = d_N \Pi_{m=1}^{N}\left[\Omega^2 - (\Omega_m^{(N)})^2\right] = 0\,, \tag{B.13}$$

whose roots $\pm\Omega_1^{(N)}$, ..., $\pm\Omega_N^{(N)}$ are approximations to the first $2N$ eigenvalues. By increasing the degree of the polynomial, $N = 1, 2, ...$, more eigenvalues are found, and better approximations are obtained, for example, the successive approximations to the fundamental frequency are $\Omega_1^{(1)}$, $\Omega_1^{(2)}$, $\Omega_1^{(3)}$, ..., which tend to the exact value

$$\Omega_1 \equiv \lim_{N\to\infty} \Omega_1^{(N)}\,. \tag{B.14}$$

This process of successive approximations is illustrated in Table 2, for the fundamental frequency and next five harmonics. For a given N, the estimate is more accurate for the fundamental frequency $\Omega_1^{(N)}$ than for the higher harmonics.